Hindawi
Mathematical Problems in Engineering
Volume 2021, Article ID 5989416, 12 pages
https://doi.org/10.1155/2021/5989416

Research Article

Simulation and Analysis of Extended Spatial Channel Model in Vehicle-to-Vehicle Communication Environments

Xin Chen,[1] **Yaolin Zhu**,[1] **and Yong Fang**[2]

[1]*School of Electronics and Information, Xi'an Polytechnic University, Xi'an 710048, China*
[2]*School of Communication and Information Engineering, Shanghai University, Shanghai, 200444, China*

Correspondence should be addressed to Xin Chen; chenxin021@shu.edu.cn

Received 24 July 2020; Accepted 30 April 2021; Published 12 May 2021

Academic Editor: Stefano Valvano

In this paper, an extension spatial channel model (SCM) for vehicle-to-vehicle (V2V) communications is proposed. To efficiently illustrate the real-world scenarios and reflect nonstationary properties of V2V channels, all effective scattering objects are subdivided into three categories of clusters according to the relative position of clusters. Besides, a birth-death process is introduced to model the appearance and disappearance of clusters on both the array and time axes. Their impacts on V2V channels are investigated via statistical properties including correlation functions. Additionally, a closed-form expression of channel impulse response (CIR) is derived from an extension SCM and cluster-based models. Furthermore, the spatial and frequency statistical properties of the reference model are thoroughly investigated. Finally, simulation results show that the proposed SCM V2V model is in close agreement with previously reported results, thereby validating the accuracy and effectiveness of the proposed model.

1. Introduction

In recent years, research into vehicle-to-vehicle (V2V) communications has gained strong momentum due to its potential in facilitating the implementation of Internet of Vehicles (IoV) and Intelligent Transportation Systems (ITS) [1, 2]. Alleviating traffic congestions and reducing potential vehicle crashes are still severe open challenges for the international community. Efficient vehicular communication is crucial for the development of ITS and requires the exchange of messages between vehicles. Moreover, V2V communication environments are expected to be one of the typical scenarios for the fifth generation (5G) wireless communication systems [2]. The performance of 5G communication systems is ultimately limited by the radio propagation channels they operate in. Therefore, it is essential to build an accurate and easy-to-use V2V channel model to describe the underlying real-world propagation channels between the transmitter (Tx) and the receiver (Rx) for 5G and 6G wireless systems [3–7].

It is well known that the set and deployment of the IEEE 802.11p standard and V2V wireless system require a solid understanding of the V2V radio propagation channel and corresponding mathematical channel characterization knowledge. This understanding can also contribute to the design and incremental improvement of effective signal processing techniques [8]. Additionally, channel modeling is expected to shed light on the real physical attenuation by investigating the channel characteristics, which is critical for developing information-enabled applications to improve traffic mobility and safety [9]. Under the scenarios of V2V communication, both Tx and Rx may be in motion and lower than scatterers on surrounding buildings. In fact, the moving scatterers, e.g., moving cars and pedestrians, have nonignorable impact on V2V channel statistics as described in [10–12]. Furthermore, the influence of changes in both angles and velocities of Tx and Rx could cause the nonstationary properties of V2V channels [13]. The performance of the V2V propagation channel between Tx and Rx can significantly differ depending on dynamic scattering

environments around them and whether the link exists line-of-sight (LoS) components owing to large obstacles, roadside infrastructures, and road bending [14]. In particular, building channel models for V2V environments are therefore of great importance for those people who are involved in the development of 5G mobile communication systems.

The different approaches to model V2V models can be roughly split into three categories: deterministic models, stochastic models, and geometry-based stochastic models (GBSMs) [9]. Due to the high computational cost of deterministic modeling and non-site-specific realization of stochastic modeling, the GBSMs are widely used in V2V communications for theoretical analysis of channel statistics and performance evaluation due to their more flexible descriptions of nonstationarities and closely reflecting real measurements of V2V channels [15]. The GBSMs can be classified as regular-shaped GBSMs (RS-GBSMs) [16–23] and irregular-shaped GBSMs [24, 25], mainly depending on whether scatterers are located on regular shapes or irregular shapes. The authors in [16–19] presented RS-GBSMs consisting two-ring [16], two-cylinder [17], and ellipse models [18, 19]. However, their underlying assumption of all scatterers is uniformly distributed on regular geometries, which does not agree with the real measurements. In [10–12], the authors investigated the fixed and moving scatterers on the statistics of MIMO V2V channels under non-line-of-sight (NLoS) scenarios where both the single- and double-bounced components were taken into account. In [26], the author proposed a V2V channel model assuming the local scatterers moving with random velocities in random directions, which is more close to the real-world scattering circumstances. Although the current RS-GBSMs can be easily changed and easily reproducing realistic temporal channel variations, there are still severe open challenges, e.g., closed-form expressions and dynamic descriptions of V2V channels [25]. Due to the obvious advantages such as based on measurements, the adaption to outdoor scattering environment in terms of mobility and the combinations of stochastic modeling and ray-based model, spatial channel model (SCM) is a widely used scheme especially in standards (e.g., ITU and 3GPP) [27, 28]. SCM is one of the standardized GBSMs, which focus on the geometry of the single- and double-bounced scatterers [29]. In [30–32], the theory of SCM is modified and employed to analytically utilize in V2V communication. Furthermore, in urban street scattering environments, the multipath components (MPCs) usually show the distribution in terms of clusters due to similar angle of arrival (AOA), angle of departure (AOD), and latency [32]. From the practical and theoretical point of view, the extended SCM provides new insights into widening the range of research on V2V modeling.

Even though many V2V channel models have been proposed over the past decade, there are still pressing needs to model V2V channels considering both the effect of randomly distributed scatterers and nonstationary property. In this regard, we extend the work described in [30, 31] by modeling nonstationary V2V fading channels. To evaluate the performance of cluster-based V2V models at specific situations that could occur, we categorize all effective clusters into three classes according to their relative location with respect to Tx and Rx: "ahead cluster," "between cluster," and "behind cluster," where each position aims to represent a particular type of physical situation, i.e., vehicles are approaching, passing, and leaving. Aside from the scatterers' aspect, realistic V2V fading channels exhibit in general nonstationarity which results in dynamic behavior of channels. Generally speaking, there are two basic manners. The first one needs the estimation of the length of time it takes for the wide-sense stationary uncorrelated scattering (WSSUS) assumption to be applicable while the other approach is based on the tapped delay line (TDL) model with the tap amplitudes following the birth-death process [30]. The literature on dynamic channel models has extensively been studied in [33–35]; there are only a few studies devoted to the statistic properties of V2V channels taking into account the position of clusters and nonstationarity (the channel statistics change). Accordingly, to the best of the authors' knowledge, the statistical properties of V2V channels in the presence of different types of clusters with dynamic channel parameters have been investigated neither analytically nor empirically so far. In this paper, we proposed an extended SCM V2V model to describe the position of clusters and dynamic cluster evolution as mobile Tx/Rx. The major contributions and novelties of this paper are summarized as follows:

(1) An extended cluster-based SCM for V2V communications is proposed. All effective scattering objects are subdivided into three categories of clusters according to the position of clusters with respect to vehicles (Tx/Rx). Three different locations between the Tx and Rx have been distinguished, which represents a particular type of physical situation, i.e., vehicles are approaching, passing, and leaving clusters. This paper focuses on the effect of locations of scatterers and nonstationary channel characterizations.

(2) To statistically model the nonstationary V2V channels, the reference model incorporates the dynamic variations of multipath components, which includes delay and angular properties as well as dynamic evolution of clusters as the Tx/Rx move. The proposed SCM V2V channel model could be useful for getting a more in-depth understanding of V2V nonstationary channel behavior.

(3) Statistical properties of the reference model are derived and investigated, including time-variant transfer function (TVTF), temporal autocorrelation function (ACF), Doppler power spectral density (PSD), and space-time-frequency correlation function (STFCF). Simulation results demonstrate the validity and effectiveness of the proposed model.

The rest of the paper is organized as follows. Section 2 briefly introduces the proposed theoretical SCM V2V channel model. The mathematical expressions of the SCM V2V channel model are presented in Section 3. The corresponding statistical properties are derived in Section 4. Numerical simulation results and analysis are presented in Section 5. Finally, a summary and conclusions in Section 6 wrap up the paper.

2. Extended SCM V2V Channel Model

In practical V2V scattering environments as shown in Figure 1, scatterers are intensively distributed in terms of clusters along the roadside since subpaths have similar AoD, AoA, and latency in a cluster [11]. Furthermore, prior studies have shown that the number and position of scatterers seriously affect the signal propagation of V2V channels [22, 26]. To efficiently analyze and design V2V systems, here all effective clusters are divided into three types according to their relative positions: "ahead cluster," "between cluster," and "behind cluster," which represent physical situations of scatterers that are located before the leading vehicle, between the vehicles, and behind the lagging vehicle, respectively. The measurement data evaluated in [36] show that more than 90% of the extracted paths consist of LoS and single-bounced scattering components, and the power of single-bounced paths is always stronger than that of double-bounced paths in a cluster. Therefore, this paper only focuses on LoS component and single-bounced components for scattering environments as illustrated in Figure 2. For ease of comprehension, it is assumed that one cluster lies on the one-hand side of the road, and both Tx and Rx move at a certain speed in the same direction. Figures 2(a)–2(c) depict a group of dense scatterers located at "ahead," "between," and "behind" of vehicles, respectively. The Tx/Rx is located at a distance (a_t/a_r) from the left-hand side of the road and at a distance (b_t/b_r) from the right-hand side of the road. The distance between Tx and Rx is denoted by D. The transmitter and receiver are equipped with M_t and M_r antenna elements, respectively. The symbols ϕ_t and ϕ_r are the AoD and AoA of LoS path without any obstruction between Tx and Rx, respectively. The model derives the AoD θ_t and AoA θ_r of single-bounced cluster. v_t and v_r denote the velocity of Tx and Rx, respectively. d_t and d_r are the distance between clusters and Tx/Rx antenna elements, respectively.

2.1. Ahead Cluster. Figure 2(a) shows that the case when the cluster is ahead of both Tx and Rx. In this setting $\theta_t, \theta_r \in (0, (\pi/2)]$, we have

$$\begin{aligned} \sin\,\theta_t &= \frac{a_t}{d_t}, \\ \sin\,\theta_r &= \frac{a_r}{d_r}, \\ \theta_r &= \arg\,\tan\left[\frac{a_r}{d_t \sin\,\theta_t - D}\right]. \end{aligned} \tag{1}$$

2.2. Between Cluster. Figure 2(b) depicts that the cluster is in the region between Tx and Rx. In this case, $\phi_t < \theta_t \le (\pi/2) \le \theta_r < \pi$, θ_r can be derived from the graph as follows:

$$\theta_r = \pi - \arg\,\tan\left[\frac{a_r}{D - d_t \cos\,\theta_t}\right]. \tag{2}$$

2.3. Behind Cluster. Figure 2(c) represents the case that the cluster is behind both Tx and Rx. In this setting, $\theta_t, \theta_r \in [(\pi/2), \pi)$, θ_r has the same mathematical expression as in that "ahead cluster" case.

3. Mathematical Expressions of SCM V2V Channel Model

3.1. Channel Impulse Response (CIR) of the Reference Model. We consider the street scattering environment in microcell urban as depicted in Figure 2. The proposed V2V model takes into account both LoS components and NLoS components, which has been up to 300 m LoS and 1 km NLoS coverage distance. The MIMO system for V2V channels can be described by a matrix $\mathbf{H}(t) = [h_{pq}(t)]_{M_t \times M_r}$ of size $M_t \times M_r$, where $p = 1, 2, \ldots, M_t$ and $q = 1, 2, \ldots, M_r$. The derived mathematical model $h_{pq}(t)$ between the p_{th} Tx antenna and the q_{th} Rx antenna can be expressed for LoS $h_{pq}^{\mathrm{LoS}}(t)$ and NLoS $h_{pq}^{\mathrm{cluster}}(t)$ cases as follows:

$$h_{pq}(t) = h_{pq}^{\mathrm{LoS}}(t) + h_{pq}^{\mathrm{cluster}}(t). \tag{3}$$

3.2. Mathematical Expressions for NLoS Components. Under NLoS conditions in the absence of LoS components, each realization consists of N clusters composed of M subpaths per cluster. The cluster component $h_{pq}^{\mathrm{cluster}}(t)$ between the p_{th} Tx antenna and the q_{th} Rx antenna can be given by (4), in which $h_{pq}^{\mathrm{ahead}}(t)$, $h_{pq}^{\mathrm{between}}(t)$, and $h_{pq}^{\mathrm{behind}}(t)$ denote the component of "ahead cluster," "between cluster," and "behind cluster," respectively.

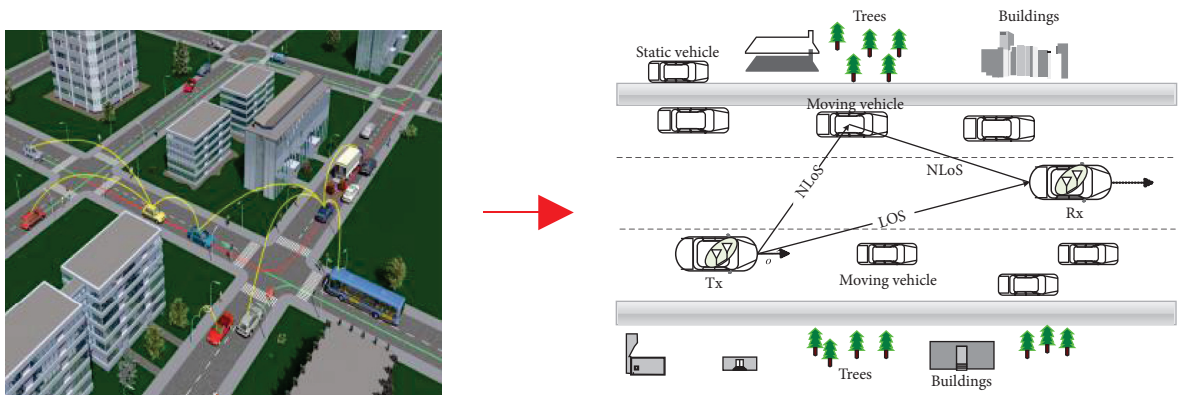

Figure 1: Geometry-based stochastic V2V channel model: (a) a typical V2V scattering scene; (b) two-dimensional V2V channel model.

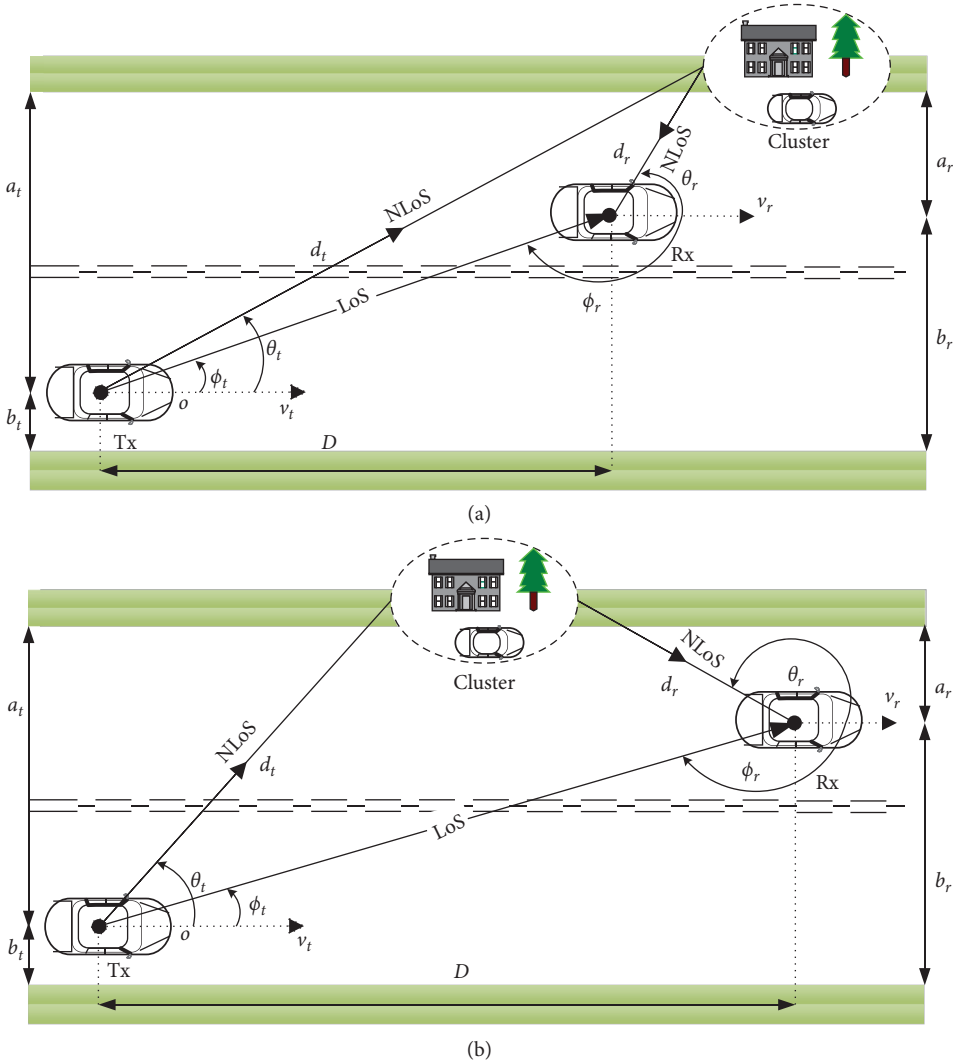

Figure 2: Continued.

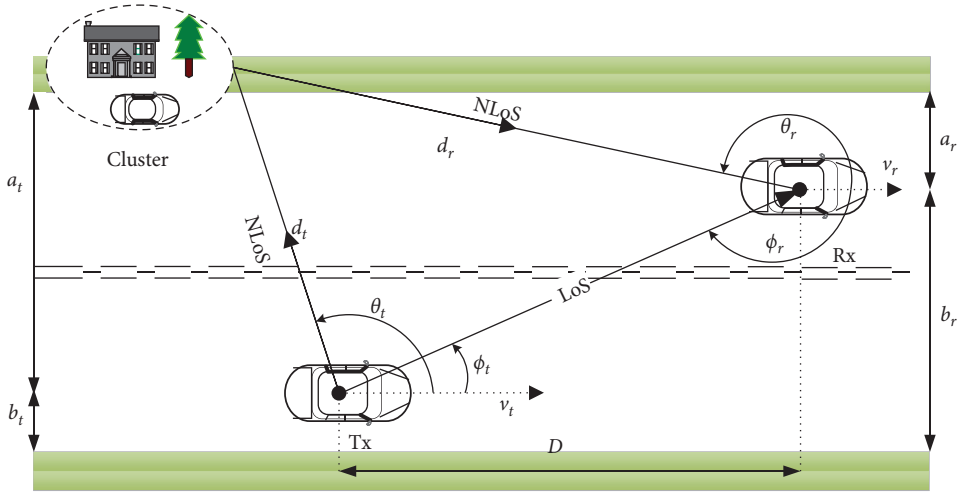

(c)

Figure 2: Three categories of clusters with respect to Tx/Rx. (a) Ahead cluster. (b) Between cluster. (c) Behind cluster.

$$
\begin{aligned}
h_{pq}^{\text{cluster}}(t) &= \sum_{i=1}^{N_a} h_{pq}^{\text{ahead}}(t) + \sum_{i=1}^{N_b} h_{pq}^{\text{between}}(t) + \sum_{i=1}^{N_c} h_{pq}^{\text{behind}}(t) \\
&= \sum_{n=1}^{N}\sum_{m=1}^{M} \sqrt{\frac{P_n}{N}}\left\{\sqrt{A_t}\,\exp\left[j\left(kd_t \sin\theta_t^{mn} + \phi_{n,m}\right)\right] \times \sqrt{A_r}\,\exp\left[j\left(kd_r \sin\theta_r^{mn}\right)\right] \times \exp\left[jk\|v\|\cos\left(\theta_r^{mn} - \theta_v\right)t\right]\right\} \\
&= \sum_{n=1}^{N}\sum_{m=1}^{M} \sqrt{\frac{P_n A_t A_r}{N}}\exp\left\{jk\left(d_t \sin\theta_t^{mn} + \phi_{n,m} + d_r \sin\theta_r^{mn} + \|v\|\cos\left(\theta_r^{mn} - \theta_v\right)t\right)\right\}.
\end{aligned}
\tag{4}
$$

The key parameters of the proposed model are summarized in Table 1. In an extreme case, there exist very dense or infinite rays of "between clusters" ($M \longrightarrow \infty$) over the interval $[0, 2\pi)$, and the component $h_{pq}^{\text{between}}(t)$ can also be regarded as

$$
\begin{aligned}
h_{pq}^{\text{between}}(t) &= \sqrt{P_n A_t A_r}\sum_{m=1}^{\infty}\exp\left\{jk\left(d_t \sin\theta_t^m + \phi_m + d_r \sin\theta_r^m + \|v\|\cos\left(\theta_r^m - \theta_v\right)t\right)\right\} \\
&= \sqrt{P_n A_t A_r}\int_0^{(\pi/2)}\exp\left\{jk\left[d_t \sin\theta_t^m + \phi_m + d_r \sin\left(g\left(\theta_t^m\right)\right) + \|v\|\cos\left(g\left(\theta_t^m\right) - \theta_v\right)t\right]\right\} p\left(\left(\theta_t^m\right)\right)\mathrm{d}\theta_t^m,
\end{aligned}
\tag{5}
$$

where

$$
g\left(\theta_t^m\right) = \pi - \arg\tan\left[\frac{a_r}{D - d_t\cos\theta_t^m}\right]. \tag{6}
$$

In (5), the function $g(\cdot)$ expresses the relationship between AoD θ_t and AoA θ_r, which can be found in (2). The probability density function (PDF) of AoD θ_t is denoted by $p(\theta_t)$. For the sake of brevity, the expressions of $h_{pq}^{\text{ahead}}(t)$ and $h_{pq}^{\text{behind}}(t)$ are omitted here.

3.3. Mathematical Expressions for LoS Components. Under LoS conditions, the CIR of SCM V2V model can be represented by (9), where ϕ_{LoS} is the phase of the LoS component, which follows the uniform distribution within $(0, 2\pi]$ and σ_s is the coefficient of lognormal shadow fading [37]. The symbol K denotes the ratio between the power of LoS paths and the power of clusters (Rician factor).

Table 1: Definition of the parameters in the V2V model.

Symbol	Definition
P_n	Power of the n_{th} cluster
N_a, N_b, N_c	Number of "ahead," "between," and "behind" clusters, respectively
N	Total number of clusters ($N = N_a + N_b + N_c$)
M	Number of subpaths per cluster
A_t, A_r	Antenna gains of Tx and Rx, respectively
M_t, M_r	Number of antennas at Tx and Rx, respectively
θ_t^{mn}	AoD of the m_{th} subpath of the n_{th} cluster
θ_r^{mn}	AoA of the m_{th} subpath of the n_{th} cluster
θ_v	Angle of Rx velocity vector
v	Relative speed of Rx velocity vector
d_t, d_r	Distance between clusters and Tx/Rx antenna elements, respectively
δ_t, δ_r	Antenna elements spacing at Tx and Rx, respectively
$\phi_{n,m}$	Phase of the m_{th} subpath of the n_{th} cluster
k	Wave number, $k = (2\pi/\lambda)$
j	Square root of -1

$$h_{pq,n=1}^{\mathrm{LoS}}(t) = \sqrt{\frac{1}{K+1}} h_{pq,1}(t) + \sigma_s \sqrt{\frac{K}{K+1}} \left\{ \begin{array}{c} \sqrt{A_t}\, \exp\left[jkd_t \sin\phi_t\right] \times \sqrt{A_r}\, \exp\left[jkd_r \sin\phi_r + \phi_{\mathrm{LoS}}\right] \\ \times \exp\left[jk\|v\|\cos\left(\phi_r - \theta_v\right)t\right] \end{array} \right\}$$
$$= \sqrt{\frac{1}{K+1}} h_{pq,1}(t) + \sigma_s \sqrt{\frac{KA_tA_r}{K+1}} \exp\{jk\left[d_t \sin\phi_t + d_r \sin\phi_r + \|v\|\cos\left(\phi_r - \theta_v\right)t\right] + \phi_{\mathrm{LoS}}\}. \tag{7}$$

Motivated by the mentioned approach in [38, 39], the MPC components are not fully resolved in time but grouped into clusters, which are particularly useful in the absence of LoS owing to dense buildings and roadside infrastructures for urban environments. Based on the above expressions of LoS components and cluster components, the CIR of the reference model at time t with delay τ can be characterized by an $M_t \times M_r$ matrix $\mathbf{H}(t,\tau) = [h_{pq}(t,\tau)]_{M_t \times M_r}$. The entries of $\mathbf{H}(t,\tau)$ consist of two parts and can be written as

$$h_{pq}(t,\tau) = \underbrace{\sqrt{\frac{K(t)}{K(t)+1}} h_{pq}^{\mathrm{LoS}}(t)\delta\left(\tau - \tau_{\mathrm{LoS}}(t)\right)}_{\mathrm{LoS}} + \underbrace{\sqrt{\frac{1}{K(t)+1}} \sum_{n=1}^{N(t)} \sum_{m_n=1}^{M_n(t)} h_{pq,n,m_n}^{\mathrm{cluster}}(t)\delta\left(\tau - \tau_n(t) - \tau_{m_n}(t)\right)}_{\mathrm{Cluster}}, \tag{8}$$

where $K(t)$ is the Rician factor, $N(t)$ denotes the time-variant number of clusters, $M_n(t)$ is the number of subpaths with n_{th} cluster, and $\tau_n(t)$ and $\tau_{m_n}(t)$ represent the delay of the n_{th} cluster and the m_{th} subpath of the n_{th} cluster. Worth pointing out is that these parameters, for any given setting, are time-variant, which has the capability to build up the dynamic and high mobility features of nonstationary V2V channels.

3.4. Array-Time Evolution for Three Types of Clusters. Let us consider the proposed channel model with multiple clusters in "ahead," "between," and "behind" three regions to describe different taps of V2V channels. There exist N total clusters, which consist of N_a "ahead" clusters, N_b "between" clusters, and N_c "behind" clusters. It is assumed that the $C_p^T(t)$ and $C_q^R(t)$ represent the cluster sets of both the p_{th} Tx antenna and the q_{th} Rx antenna at time t, which are generated based on the birth-death process on both array and time axes [29]. Then, the total number of clusters $N(t)$ observable by both Tx and Rx at time t can be expressed as

$$N(t) = \mathrm{card}\left(\bigcup_{p=1}^{M_t} \bigcup_{q=1}^{M_r} \left(C_p^T(t) \cap C_q^R(t) \right) \right), \tag{9}$$

where $\mathrm{card}(\Omega)$ denotes the cardinality of the set Ω. The symbols $\cup$ and $\cap$ are the union and intersection of sets, respectively. The generation rate and recombination rate of clusters between the Tx and the Rx are denoted by λ_G and λ_R (per meter). Such a generation-recombination behavior of clusters can be given by Poisson processes. It is assumed that the interval between time instants t_k is smaller than the coherence time of V2V channels. At any time instant t_k, it can be distinguished between newly generated clusters and the previous existing clusters at time instant t_{k-1}. Therefore, the expectation for the total number of clusters can be calculated as

$$E[N] = \frac{\lambda_G}{\lambda_R}, \tag{10}$$

where $E[\cdot]$ designates the expectation. The mean power of a generated cluster is extended to compute the mean power of subpaths within a cluster as

$$P_n = \exp\left(-\tau_{n_m} \frac{r_\tau - 1}{E\left[\tau_{n_m}\right]} \right) 10^{-\left(Z_{n,m}/10\right)}, \tag{11}$$

where $Z_{n,m}$ follows a Gaussian distribution $\mathcal{N}(0,3)$ and r_τ is the delay scalar. The survival probabilities of the clusters on

array axis at the "ahead" P^A_{survial}, "between" P^B_{survial}, and "behind" P^C_{survial} location can be given by

$$P^A_{\text{survival}} = e^{-\lambda_R \xi_a}, \tag{12}$$

$$P^C_{\text{survival}} = e^{-\lambda_R \xi_c}, \tag{13}$$

$$P^B_{\text{survival}} = e^{-\lambda_R \xi_b}, \tag{14}$$

where ξ_a, ξ_b, and ξ_c are the scenario-dependent correlation factor at "ahead," "between," and "behind" region, respectively, which are related to movements of Tx/Rx and locations of scatterers. The higher the values of ξ_i, the more reduced the correlation factor would be. A proper description for such a birth-death behavior that clusters appear, remain, and disappear is given by Poisson processes in [38]. Therefore, the average number of newly generated clusters N^{new}_a, N^{new}_b, and N^{new}_c is generated according to a Poisson distribution with expectation

$$\begin{aligned} E\left[N^{\text{new}}_a\right] &= \frac{\lambda_G}{\lambda_R}\left(1 - e^{-\lambda_R \xi_a}\right), \\ E\left[N^{\text{new}}_b\right] &= \frac{\lambda_G}{\lambda_R}\left(1 - e^{-\lambda_R \xi_b}\right), \\ E\left[N^{\text{new}}_c\right] &= \frac{\lambda_G}{\lambda_R}\left(1 - e^{-\lambda_R \xi_c}\right). \end{aligned} \tag{15}$$

To describe the cluster evolution on the time axis, we define the time-dependent channel fluctuations $q(t + \triangle t)$ in the time span between t and $t + \triangle t$. The channel fluctuations are mainly caused by movements of Tx/Rx and scatterers. Therefore, the channel fluctuation function can be defined by [38]

$$q(t + \triangle t) = q_a(t + \triangle t) + q_b(t + \triangle t) + q_c(t + \triangle t), \tag{16}$$

where $q_a(t + \triangle t)$, $q_b(t + \triangle t)$, and $q_c(t + \triangle t)$ are the channel fluctuations caused by the movement of "ahead," "between," and "behind" clusters, respectively, which are given by

$$\begin{aligned} q_a(t + \triangle t) &= P_{Fa}\left(\left\|v^a_t\right\| + \left\|v^a_r\right\|\right)\triangle t, \\ q_b(t + \triangle t) &= P_{Fb}\left(\left\|v^b_t\right\| + \left\|v^b_r\right\|\right)\triangle t, \\ q_c(t + \triangle t) &= P_{Fc}\left(\left\|v^c_t\right\| + \left\|v^c_r\right\|\right)\triangle t, \end{aligned} \tag{17}$$

where P_{Fa}, P_{Fb}, and P_{Fc} are the percentage of moving "ahead," "between," and "behind" clusters, respectively. The velocity vectors v^a_t and v^a_r are the relative speed of "ahead" cluster to Tx and Rx, respectively. For the sake of brevity, other velocity parameters are omitted here for similar situations as "ahead" case. Given the scenario-dependent correlation factor ξ_i, the survival probability P_{survival} in the time span can be calculated as [29]

$$\begin{aligned} P_{\text{survival}}\left[q_a(t + \triangle t)\right] &= e^{-\left(\lambda_R q_a (t+\triangle t)/\xi_a\right)}, \\ P_{\text{survival}}\left[q_b(t + \triangle t)\right] &= e^{-\left(\lambda_R q_b (t+\triangle t)/\xi_b\right)}, \\ P_{\text{survival}}\left[q_c(t + \triangle t)\right] &= e^{-\left(\lambda_R q_c (t+\triangle t)/\xi_c\right)}. \end{aligned} \tag{18}$$

The number of newly generated clusters at time instant $t + \triangle t$ can be calculated according to a Poisson distribution with expectation

$$\begin{aligned} E\left[N^{\text{new}}_a(t + \triangle t)\right] &= \frac{\lambda_G}{\lambda_R}\left(1 - e^{-\left(\lambda_R q_a (t+\triangle t)/\xi_a\right)}\right), \\ E\left[N^{\text{new}}_b(t + \triangle t)\right] &= \frac{\lambda_G}{\lambda_R}\left(1 - e^{-\left(\lambda_R q_b (t+\triangle t)/\xi_b\right)}\right), \\ E\left[N^{\text{new}}_c(t + \triangle t)\right] &= \frac{\lambda_G}{\lambda_R}\left(1 - e^{-\left(\lambda_R q_c (t+\triangle t)/\xi_c\right)}\right). \end{aligned} \tag{19}$$

The process of the newly generated cluster observed at both Tx and Rx antennas can be summarized in Table 2.

4. Statistical Properties of the Proposed SCM V2V Channel Model

4.1. Time-Variant Transfer Function. The time-variant transfer function (TVTF) $H_{pq}(t, f)$ is the Fourier transform of CIR $h_{pq}(t)$ with respect to delay, which can be expressed as

$$\begin{aligned} H_{pq}(t, f) = \int_{-\infty}^{\infty} h_{pq}(t) e^{-j2\pi f \tau} \mathrm{d}\tau &= \sqrt{\frac{K}{K+1}} h^{\text{LoS}}_{pq}(t) e^{-j2\pi f \tau_{\text{LoS}}(t)} \\ &+ \sqrt{\frac{1}{K+1}} \sum_{n=1}^{N(t)} \sum_{m_n=1}^{M_n(t)} h^{\text{cluster}}_{pq,n,m_n} e^{-j2\pi f \left(\tau_n(t) + \tau_{m_n}\right)}, \end{aligned} \tag{20}$$

where f denotes the frequency.

4.2. Temporal Autocorrelation Function. To illustrate the effect of clusters on the temporal autocorrelation function (ACF) of the proposed model, the expression of ACF $\rho_{pq}(\Delta t; t)$ is derived as

$$\rho_{pq}(\Delta t; t) = E\left[\frac{h^*_{pq}(t) h_{pq}(t + \Delta t)}{\left|h^*_{pq}(t)\right\| h_{pq}\left(t + \Delta t\right)\right|}\right] = \rho^{\text{LoS}}_{pq}(\Delta t; t) + \rho^{\text{cluster}}_{pq}(\Delta t; t), \tag{21}$$

where $(\cdot)^*$ denotes the complex conjugate operation. Since the LoS and cluster components are independent of each other, and there are no correlations between the underlying processes in different taps, therefore, we have the following ACF:

Table 2: The process of newly generated clusters.

Step	Description
1	Generate initial indices $\widetilde{p}$ $(1 \le \widetilde{p} \le M_t)$ and $\widetilde{q}$ $(1 \le \widetilde{q} \le M_r)$ for the Tx and the Rx antenna arrays
2	Evolve the cluster at the Tx antenna from 1 − st to $(\widetilde{p}-1)$ − th and from $(\widetilde{p}+1)$ − th to M_t − th antenna
3	Evolve the cluster at the Rx antenna from 1 − st to $(\widetilde{q}-1)$ − th and from $(\widetilde{q}+1)$ − th to M_r − th antenna
4	Update the cluster sets observed at both the Tx and the Rx antennas

$$\rho_{pq}^{\mathrm{LoS}}(\Delta t;t) = e^{\left\{jk\|v\|\cos\left(\phi_r-\theta_v\right)\Delta t+2\phi_{\mathrm{LoS}}\right\}},$$
$$\rho_{pq}^{\mathrm{cluster}}(\Delta t;t) = \sum_{n=1}^{N}\sum_{m=1}^{M} e^{\left\{jk\|v\|\cos\left(\theta_r^{mn}-\theta_v\right)\Delta t\right\}}. \tag{22}$$

4.3. Doppler Power Spectral Density. The Doppler power spectral density (PSD) $S(f;t)$ with respect to the Doppler frequency f can be obtained by the Fourier transform of the temporal ACF, which can be calculated as

$$\begin{aligned} S(f;t) &\coloneqq \int_{-\infty}^{\infty} \rho_{pq}(\Delta t;t)e^{-j2\pi f\Delta t}\mathrm{d}(\Delta t) \\ &= \int_{-\infty}^{\infty} \rho_{pq}^{\mathrm{LoS}}(\Delta t;t)e^{-j2\pi f\Delta t}\mathrm{d}(\Delta t) \\ &\quad + \int_{-\infty}^{\infty} \rho_{pq}^{\mathrm{cluster}}(\Delta t;t)e^{-j2\pi f\Delta t}\mathrm{d}(\Delta t). \end{aligned} \tag{23}$$

It is noteworthy that the Doppler PSD is time t dependent. Substituting (12) and (13) into (14), the PSD can be expressed as

$$\begin{aligned} S(f;t) &= \int_{-\infty}^{\infty} e^{j\left[k\|v\|\cos\left(\phi_r-\theta_v\right)-2\pi f\right]\Delta t+2\phi_{\mathrm{LoS}}}\mathrm{d}(\Delta t) \\ &\quad + \int_{-\infty}^{\infty}\int_{0}^{\pi} e^{j\left[k\|v\|\cos\left(\theta_r^{mn}-\theta_v\right)-2\pi f\right]\Delta t}\mathrm{d}\theta_r^{mn}\mathrm{d}(\Delta t). \end{aligned} \tag{24}$$

4.4. Space-Time-Frequency Correlation Function. The normalized space-time-frequency correlation function (STFCF) between time-variant transfer functions $h_{pq}(f,t)$ and $h_{p'q'}(f,t)$ is defined as [40–42]

$$\begin{aligned} R_{pq,p'q'}(\Delta t;\Delta f) &= \frac{E\left[H_{pq}^{*}(t,f)H_{p'q'}(t+\Delta t,f+\Delta f)\right]}{\sqrt{E\left[\left|H_{pq}(t,f)\right|^2\right]E\left[\left|H_{p'q'}(t,f)\right|^2\right]}} \\ &= R_{pq,p'q'}^{\mathrm{LoS}}(\Delta t;\Delta f) + R_{pq,p'q'}^{\mathrm{cluster}}(\Delta t;\Delta f). \end{aligned} \tag{25}$$

For the sake of simplicity, we assume that the relative delays and Rician factor are constants at time instant t, i.e., $K(t) = K$, $\tau_n(t) = \tau_n$, and $\tau_{m_n}(t) = \tau_{m_n}$. Substituting (20) into (25), we can get the expressions of $R_{pq,p'q'}^{\mathrm{LoS}}(\Delta t;\Delta f)$ and $R_{pq,p'q'}^{\mathrm{cluster}}(\Delta t;\Delta f)$ as the following formula:

$$R_{pq,p'q'}^{\mathrm{LoS}}(\Delta t;\Delta f) = e^{j\left\{k\|v\|\cos\left(\phi_r-\theta_v\right)\Delta t-2\pi\Delta f\tau_{\mathrm{LoS}}\right\}}, \tag{26}$$

$$R_{pq,p'q'}^{\mathrm{cluster}}(\Delta t;\Delta f) = \sum_{n=1}^{N}\sum_{m=1}^{M} e^{j\left\{k\|v\|\cos\left(\theta_r^{mn}-\theta_v\right)\Delta t-2\pi\Delta f\left[\tau_n+\tau_{m_n}\right]\right\}}. \tag{27}$$

5. Simulation Results and Analysis

5.1. Model Parameter Selection. In the simulations, the proposed extended SCM V2V channel model has been implemented in the common environment (Table 1 in [38]), which contributes to an easier physical understanding of simulations. Considering the movement of Tx and Rx as well as channel fluctuations, the time-variant parameters of CIR are generated. The radio propagation environment contains moving scatterers and fixed scatterers, which are distributed in three regions along the roadside. Each realization contains 20 clusters and 10 subpaths per cluster. For simplicity purposes, both Tx and Rx have the same speed in the same direction. The following parameters were chosen as $\delta_t = \delta_r = 0.5\lambda$, $A_t = A_r = 1$, $K = 2, M_t = M_r = 2$. Some parameters are chosen based on reasonable assumptions: the distances of subpaths per cluster between Tx and Rx are all set to 1 km. For subpaths of a cluster, the AoD θ_t^{mn} and AoA θ_r^{mn} are stochastically distributed at the center of cluster angle over these three regions:

(i) "Ahead cluster" angles: $\theta_t^{mn} = 30^\circ, \theta_r^{mn} = 60^\circ$

(ii) "Between cluster" angles: $\theta_t^{mn} = 30^\circ, \theta_r^{mn} = 120^\circ$

(iii) "Behind cluster" angles: $\theta_t^{mn} = 120^\circ, \theta_r^{mn} = 150^\circ$

The standard deviations are less than one degree. Considering the angles of subpaths in a cluster within the differential angle $(\Delta\theta_t^{mn} \le 1^\circ, \Delta\theta_r^{mn} \le 1^\circ)$ with respect to their neighboring subpaths, the radius of each cluster is 50 m and is independent with its neighboring clusters.

5.2. ACF and PSD of the Reference Model. Figure 3 shows the ACF curves of different clusters in three scattering regions. The speed of moving scatterers, Tx, and Rx are denoted as v_s, v_t, and v_r, respectively. It is observed that the ACF changes more slowly as the speed of moving scatterers decreases. The higher the moving speed v_s, the more rapidly the curve drops. One common understanding is that when the Δt exceeds the threshold of about 5 ms, the value of ACF tends

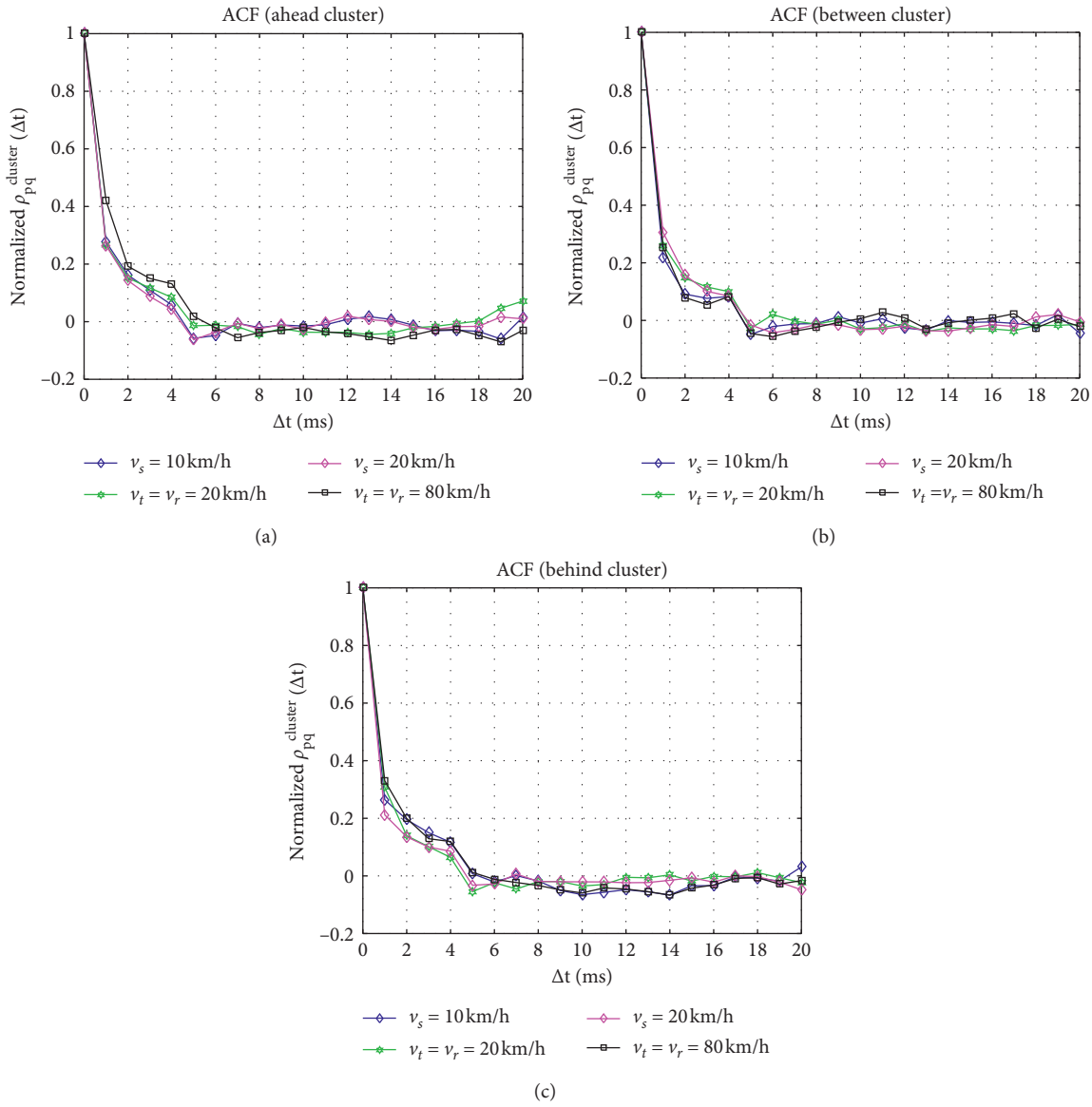

Figure 3: ACF for three categories of clusters in different regions (note: the average velocities of moving scatterers v_s are set to 10 (km/h) and 20 (km/h) and the speed of mobile terminals Tx/Rx (v_t/v_r) are set to 20 (km/h) and 80 (km/h) in each scene.). (a) ACF for ahead clusters. (b) ACF for between clusters. (c) ACF for behind clusters.

to be around zero, which contributes to calculate the coherent time of V2V channels in different scenarios. Worth pointing out is that these coherent time values are, for any given setting, theoretical analysis of channel statistics and performance evaluation; hence, we cannot expect to glean from them all that is consistent with the real measurements. Due to the moving speeds of scatterers and Tx/Rx involved, V2V channels show strong time variance, while positions of clusters have less effect on the overall tendency of ACF profile. The correlations between ACF and PSD are Fourier transform pair, and the PSD for between clusters is presented in Figure 4. It is found that the PSD is sensitive to the velocities of mobile terminals. Furthermore, the faster the mobile user, the greater the cutoff frequency would be.

5.3. STFCF of the Reference Model. Figure 5 depicts the absolute value of STFCF for ahead cluster, between cluster, and behind cluster. A good agreement can be shown in Figures 5(a)–5(c), which illustrates that the positions of ahead clusters have a weak correlation with STFCF. This is due to the fact that STFCF is the function of time delay τ_n and τ_{m_n} in (25) and (26), respectively. Worth pointing out is that time delay τ can be calculated by $\tau = \tau_n + \tau_{m_n}$ in

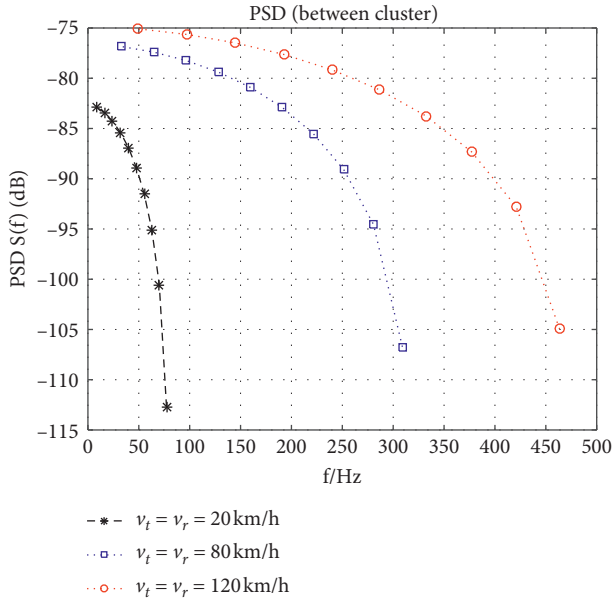

Figure 4: Behavior of PSD presented in Figure 2(b) for "between cluster" scenario.

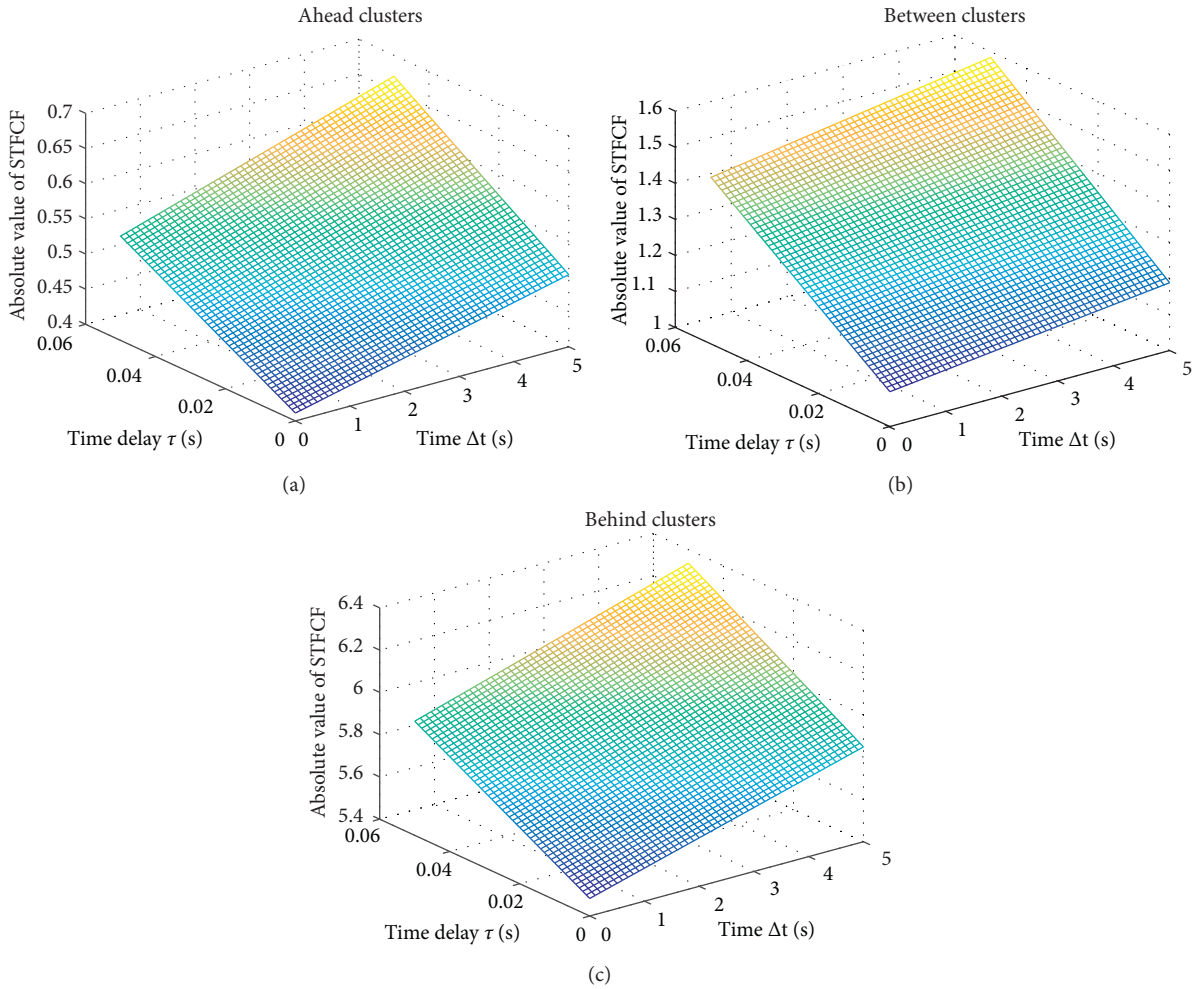

Figure 5: The absolute value of STFCF for clusters in different regions. (a) STFCF for ahead clusters. (b) STFCF for between clusters. (c) STFCF for behind clusters.

Figure 5. The curve of STFCF for behind cluster is the maximum value comparing with other cases. The AoD and AoA are also important factors in estimating the overall tendency of STFCF by numerical simulations.

6. Conclusion

This paper explores an extension SCM V2V channel model. We describe the channel characteristics of both LoS and single-bounced clusters. Furthermore, this paper further analyzes the dynamics of clusters by introducing a birth-death process. Based on this model, we have derived the mathematical expressions of channel characteristics. By assuming an isotropic single-bounced scattering scenario, simulation results show the relationships between correlation functions and the locations of different clusters. We have pointed out the calculation methods of coherent time for V2V channels in different scattering scenarios.

Data Availability

The data used to support the findings of this study are available from the corresponding author upon request.

Conflicts of Interest

The authors declare that they have no conflicts of interest.

Acknowledgments

This work was supported by the National Natural Science Foundation of China under Grant no. 61673253, the Chinese Postdoctoral Science Foundation under Grant no. 2020M683562, the Specialized Research Fund for Xi'an University Talent Service Enterprise Project under Grant no. GXYD7.11, the Special Scientific Research Project of Shaanxi Provincial Department of Education under Grant no. 20JK0645, and the Specialized Research Fund for Shaoxing Keqiao West-Tex Textile Industry Innovative Institute Project under Grant no. 19KQYB11.

References

[1] B. Ji, X. Zhang, S. Mumtaz et al., "Survey on the Internet of Vehicles: network architectures and applications," *IEEE Communications Standards Magazine*, vol. 4, no. 1, pp. 34–41, 2020.

[2] S. Wu, C.-X. Wang, e.-H. M. Aggoune, M. M. Alwakeel, and X. You, "A general 3-D non-stationary 5G wireless channel model," *IEEE Transactions on Communications*, vol. 66, no. 7, pp. 3065–3078, 2018.

[3] J. S. Wey, Y. Luo, and T. Pfeiffer, "5G wireless transport in a PON context: an overview," *IEEE Communications Standards Magazine*, vol. 4, no. 1, pp. 50–56, 2020.

[4] H. Jiang, M. Mukherjee, J. Zhou, and J. Lloret, "Channel modeling and characteristics for 6G wireless communications," *IEEE Network*, vol. 35, no. 1, pp. 296–303, 2021.

[5] Z. Huang and X. Cheng, "A general 3D space-time-frequency non-stationary model for 6G channels," *IEEE Transactions on Wireless Communications*, vol. 20, no. 1, pp. 535–548, 2021.

[6] V. Marojevic, I. Guvenc, R. Dutta, M. L. Sichitiu, and B. A. Floyd, "Advanced wireless for unmanned aerial systems: 5G standardization, research Challenges, and AERPAW architecture," *IEEE Vehicular Technology Magazine*, vol. 15, no. 2, pp. 22–30, 2020.

[7] R. M. Masegosa and J. Gozalvez, "LTE-V for sidelink 5G V2X vehicular communications: a new 5G technology for short-range vehicle-to-everything communications," *IEEE Communications Surveys & Tutorials*, vol. 12, no. 4, pp. 30–39, 2017.

[8] H. Jiang, Z. Zhang, J. Dang, and L. Wu, "A novel 3-D massive MIMO channel model for vehicle-to-vehicle communication environments," *IEEE Transactions on Communications*, vol. 66, no. 1, pp. 79–90, 2018.

[9] Y. Li, C. X. Wang, Y. J. He et al., "3D wideband non-stationary geometry-based stochastic models for non-isotropic MIMO vehicle-to-vehicle channels," *IEEE Trans. on Wireless Communications*, vol. 14, no. 12, pp. 6883–6895, 2015.

[10] C. Huang, R. Wang, P. Tang et al., "Geometry-cluster-based stochastic MIMO model for vehicle-to-vehicle communications in street canyon scenarios," *IEEE Transactions on Wireless Communications*, vol. 20, no. 2, pp. 755–770, 2021.

[11] X. Chen, Y. Fang, W. Xiang, and L. Zhou, "Research on spatial channel model for vehicle-to-vehicle communication channel in roadside scattering environment," *International Journal of Antennas and Propagation*, vol. 2017, Article ID 3098198, 12 pages, 2017.

[12] A. G. Zajić, "Impact of moving scatterers on vehicle-to-vehicle narrow-band channel characteristics," *IEEE Trans. on Vehicular Technology*, vol. 63, no. 7, pp. 3904–3106, 2014.

[13] W. Dahech, M. Pätzold, C. A. Gutierrez, and N. Youssef, "A non-stationary mobile-to-mobile channel model allowing for velocity and trajectory variations of the mobile stations," *IEEE Transactions on Wireless Communications*, vol. 16, no. 3, pp. 1987–2000, 2017.

[14] M. Riaz, N. M. Khan, and S. J. Nawaz, "A generalized 3-D scattering channel model for spatiotemporal statistics in mobile-to-mobile communication environment," *IEEE Transactions on Vehicular Technology*, vol. 64, no. 10, pp. 4399–4410, 2015.

[15] M. Walter, D. Shutin, and U.-C. Fiebig, "Delay-dependent Doppler probability density functions for vehicle-to-vehicle scatter channels," *IEEE Transactions on Antennas and Propagation*, vol. 62, no. 4, pp. 2238–2249, 2014.

[16] X. Zhao, X. Liang, S. Li, and K. Haneda, "Mobile-to-mobile wideband MIMO channel realization by using a two-ring geometry-based stochastic scattering model," *Wireless Personal Communications*, vol. 84, no. 4, pp. 2445–2465, 2015.

[17] X. Zhao, X. Liang, S. Li, and B. Ai, "Two-cylinder and multi-ring GBSSM for realizing and modeling of vehicle-to-vehicle wideband MIMO channels," *IEEE Transactions on Intelligent Transportation Systems*, vol. 17, no. 10, pp. 2787–2799, 2016.

[18] X. Liang, X. Zhao, Y. Li, S. Li, and Q. Wang, "A non-stationary geometry-based street scattering model for vehicle-to-vehicle wideband MIMO channels," *Wireless Personal Communications*, vol. 90, no. 1, pp. 325–338, 2016.

[19] R. B. Ertel and J. H. Reed, "Angle and time of arrival statistics for circular and elliptical scattering models," *IEEE Journal on Selected Areas in Communications*, vol. 17, no. 11, pp. 1829–1840, 1999.

[20] Y. Yuan, C.-X. Wang, X. Cheng, B. Ai, and D. I. Laurenson, "Novel 3D geometry-based stochastic models for non-isotropic MIMO vehicle-to-vehicle channels," *IEEE Transactions on Wireless Communications*, vol. 13, no. 1, pp. 298–309, 2014.

[21] X. Cheng, C.-X. Wang, D. Laurenson, S. Salous, and A. Vasilakos, "An adaptive geometry-based stochastic model for non-isotropic MIMO mobile-to-mobile channels," *IEEE Transactions on Wireless Communications*, vol. 8, no. 9, pp. 4824–4835, 2009.

[22] N. Avazov and M. Pätzold, "A novel wideband MIMO car-to-car channel model based on a geometrical semi-circular tunnel scattering model," *IEEE Transactions on Vehicular Technology*, vol. 65, no. 3, pp. 1070–1082, 2016.

[23] S. J. Nawaz, M. Riaz, N. M. Khan, and S. Wyne, "Temporal analysis of a 3D ellipsoid channel model for the vehicle-to-vehicle communication environments," *Wireless Personal Communications*, vol. 82, no. 3, pp. 1337–1350, 2015.

[24] C. X. Wang, X. Cheng, and D. Laurenson, "Vehicle-to-vehicle channel modeling and measurements: recent advances and future challenges," *IEEE Communications Magazine*, vol. 47, no. 11, pp. 96–103, 2009.

[25] X. Cai, B. Peng, X. Yin, and A. P. Yuste, "Hough-transform-based cluster identification and modeling for V2V channels based on measurements," *IEEE Transactions on Vehicular Technology*, vol. 67, no. 5, pp. 3838–3852, 2018.

[26] A. Borhani and M. Pätzold, "Correlation and spectral properties of vehicle-to-vehicle channels in the presence of moving scatterers," *IEEE Transactions on Vehicular Technology*, vol. 62, no. 9, pp. 4228–4239, 2013.

[27] "Spatial channel model for multiple input multiple output (MIMO) simulations," Technical report, 2011.

[28] Y. Wang, Z. Shi, L. Huang, Z. Yu, and C. Cao, "An extension of spatial channel model with spatial consistency," in *Proceedings of the 2016 IEEE 84th Vehicular Technology Conference (VTC-Fall)*, Montreal, Canada, Sepetember 2016.

[29] S. Wu, C.-X. Wang, e.-H. M. Aggoune, M. M. Alwakeel, and Y. He, "A non-stationary 3-D wideband twin-cluster model for 5G massive MIMO channels," *IEEE Journal on Selected Areas in Communications*, vol. 32, no. 6, pp. 1207–1218, 2014.

[30] A. B. Al-Khalil, S. Turner, and A. Al-Sherbaz, "Feasibility study of utilising SCM-MIMO channel model in V2V communication," in *Proceedings of the 7th International Workshop On Communication Technologies For Vehicles*, St.-Petersburg, Russia, October 2014.

[31] A. B. Al-Khalil, S. Turner, and A. Al-Sherbaz, "Utilising SCM-MIMO channel model based on V-blast channel coding in V2V communication," in *Proceedings of the 8th International Workshop On Communication Technologies For Vehicles*, pp. 3–11, Sousse, Tunisia, May 2015.

[32] Y. Li, R. He, S. Lin et al., "Cluster-based nonstationary channel modeling for vehicle-to-vehicle communications," *IEEE Antennas and Wireless Propagation Letters*, vol. 16, pp. 1419–1422, 2017.

[33] W. Wang, T. Jost, U. Fiebig, and W. Koch, "Time-variant channel modeling with application to mobile radio based positioning," in *Proceedings of the IEEE GLOBECOM*, pp. 5038–5043, Anaheim, CA, USA, December 2012.

[34] M. L. Jakobsen, T. Pedersen, and B. H. Fleury, "Analysis of stochastic radio channels with temporal birth-death dynamics: a marked spatial point process perspective," *IEEE Transactions on Antennas and Propagation*, vol. 62, no. 7, pp. 3761–3775, 2014.

[35] R. He, O. Renaudin, V.-M. Kolmonen et al., "A dynamic wideband directional channel model for vehicle-to-vehicle communications," *IEEE Transactions on Industrial Electronics*, vol. 62, no. 12, pp. 7870–7882, 2015.

[36] J. H. Zhao, Y. Chen, and Y. Gong, "Study of connectivity probability of vehicle-to-vehicle and vehicle-to-infrastructure communication systems," in *Proceedings of the IEEE 83rd Vehicluar Technology Conference*, Nanjing, China, May 2016.

[37] A. B. Al-Khalil, S. Turner, and A. Al-Sherbaz, "A predefined channel coefficients library for vehicle-to-vehicle communications," in *Proceedings of the 7th International Workshop on Reliable Networks Design And Modeling*, pp. 335–340, Munich, Germany, October 2015.

[38] T. Zwick, C. Fischer, D. Didascalou, and W. Wiesbeck, "A stochastic spatial channel model based on wave-propagation modeling," *IEEE Journal on Selected Areas in Communications*, vol. 18, no. 1, pp. 6–15, 2000.

[39] T. Zwick, C. Fischer, and W. Wiesbeck, "A stochastic multipath channel model including path directions for indoor environments," *IEEE Journal on Selected Areas in Communications*, vol. 20, no. 6, pp. 1178–1192, 2002.

[40] P. Kyosti, J. Meinila, and L. Hentila, "WINNER II channel model," Technical report IST-4-027756, 2008.

[41] A. Zajić and G. Stüber, "Statistical properties of wideband MIMO mobile-to-mobile channels," in *Proceedings of the 2008 IEEE Wireless Communications and Networking Conference (WCNC)*, pp. 763–768, Las Vegas, NV, USA, April 2008.

[42] A. G. Zajic and G. Stüber, "Three-dimensional modeling and simulation of wideband MIMO mobile-to-mobile channels," *IEEE Transactions on Wireless Communications*, vol. 8, no. 3, pp. 1260–1275, 2009.